Effect of contact geometry on spin-transport signals in nonlocal (Ga,Mn)As/GaAs devices

M. Ciorga,* M. Utz, D. Schuh, D. Bougeard, and D. Weiss
Experimentelle und Angewandte Physik, University of Regensburg, D-93040 Regensburg, Germany
(Received 29 July 2013; published 9 October 2013)

We report on spin-valve experiments in lateral spin-injection devices with different geometries of (Ga,Mn)As/GaAs spin Esaki diode contacts. We study the influence of the geometry of the contacts, i.e., their widths and the crystallographic orientation, on the magnetization reversal process and the resulting pattern observed in the spin-valve signal. We find that tuning of the magnetic anisotropy of the narrow (Ga,Mn)As stripes by means of lithographically induced anisotropic strain relaxation allows one to realize parallel, antiparallel, and even orthogonal configurations of magnetizations in injector and detector contacts. Understanding of the switching between these configurations during sweeping of the external in-plane magnetic field is crucial for a proper interpretation of the measured nonlocal spin signals.

DOI: 10.1103/PhysRevB.88.155308 PACS number(s): 72.25.Hg, 75.50.Pp, 75.60.Jk

I. INTRODUCTION

The efficient generation and subsequent detection of spin accumulation in nonmagnetic semiconductors is a fundamental issue in semiconductor spintronics. Recent years have seen substantial progress on all-electrical spin injection and detection in lateral semiconductor devices with GaAs-based,[1,2] Si,[3] and Ge[4] bulk transport channels. The discovery of a ferromagnetism in semiconductor materials[5,6] made the realization of all-semiconductor spin-injection devices possible, with a ferromagnetic (Ga,Mn)As layer employed, in Esaki diode configuration, as a source of spin polarized electrons.[7–11] Electrical spin injection and detection in lateral devices is typically realized in a so-called nonlocal (NL) configuration,[1,2,12] where spin accumulation is generated in the channel by means of a charge current flowing from the injector contact into the channel and is detected by a second contact, placed in the close vicinity of the injector, outside the current path. Detection is demonstrated by means of a spin-valve (SV) effect, where the changes in the nonlocal voltage measured at the detector are observed as a result of switching between parallel and antiparallel orientation of magnetization in the injector and detector during the magnetic reversal process induced by in-plane magnetic field sweeps. In one of our previous works on lateral devices with (Ga,Mn)As/GaAs contacts[2] we showed, however, that parallel-antiparallel (P-AP) switching of magnetization configuration was not required to observe a spin-valve-like pattern in the nonlocal voltage. As the analysis of the measured spin signals is typically based on the assumption of P-AP switching, understanding of the switching behavior of ferromagnetic contacts is crucial for a proper interpretation of the data. In this paper we therefore investigate the nonlocal spin-valve (NLSV) effect in such devices in more details. We study the evolution of the signal in dependence on the geometry of the contacts, i.e., their size and crystallographic orientation. We find that parallel, antiparallel, and even orthogonal configurations of magnetizations in injector and detector contacts are possible, leading to different spin-valve patterns.

The paper is organized as follows. In Sec. II we shortly discuss magnetic anisotropies characteristic of (Ga,Mn)As. In Sec. III we describe our experimental devices and the main experimental methods we use, i.e., the spin-valve effect and the Hanle effect. In Sec. IV we present and discuss the results of experiments on contacts oriented along [100], as well as along $[1\bar{1}0]$ directions. We conclude with Sec. V, where we give a summary of our findings.

II. MAGNETIC ANISOTROPY IN (Ga,Mn)As.

(Ga,Mn)As is known to have very rich anisotropy features.[13,14] From the symmetry rules for zinc blend structure materials one expects for bulk (Ga,Mn)As a cubic magnetocrystalline anisotropy with three equivalent easy axes either along ⟨100⟩ or ⟨111⟩ directions. For the epitaxially grown material this anisotropy is strongly influenced both by the growth direction and the substrate material. The majority of studied (Ga,Mn)As films (including the ones studied in this work) are grown on (001) substrates, resulting in cubic easy axes along ⟨100⟩ directions. The lattice mismatch between the (Ga,Mn)As film and the substrate induces a biaxial strain in the plane of the film, which breaks the cubic symmetry and leads to a uniaxial anisotropy perpendicular to the layer. The sign of the anisotropy depends on the sign of the strain: Tensile strain (e.g., InGaAs as a substrate) leads to an easy axis perpendicular to the plane,[15] whereas the compressive strain (GaAs as a substrate), for samples with high hole concentrations, typically used in transport experiments, leads to an easy axis in the plane of the film.[16] Additionally to the cubic in-plane (biaxial) anisotropy there is also a uniaxial in-plane anisotropy along the ⟨110⟩ directions present, breaking the equivalence of [110] and $[1\bar{1}0]$ directions. The origin of this anisotropy is still not fully understood, although it was recently suggested that the anisotropic arrangement of Mn atoms on the growth surface can be responsible for a reduction in the symmetry of the system.[17] In some (Ga,Mn)As samples another small, and not yet understood, uniaxial anisotropy component is observed, breaking the equivalence between [100] and [010] directions.[18,19]

The anisotropy features discussed above have a profound effect on how the magnetization of (Ga,Mn)As film reverses its orientation during magnetic field sweeps between saturation values in opposite directions of the B field. It was shown that biaxial anisotropy leads to a double step reversal process through nucleation and propagation of 90° domain walls,[18] in a similar way as was observed before for Fe films.[20]

Anisotropy properties of (Ga,Mn)As are modified when films are patterned into narrow stripes, like in spintronics microdevices. Contrary to the metal ferromagnets, however, the changes are not induced by shape anisotropy, which usually fixes the magnetic easy axis of a ferromagnetic stripe along its longest geometrical axis. The reason is that the shape anisotropy is proportional to the saturation magnetization of the material, which is quite small for such a diluted ferromagnet as (Ga,Mn)As. It was shown, however, that the geometry of the (Ga,Mn)As stripes also influences the anisotropy features in a similar way as shape anisotropy does in metal ferromagnets. The origin of the observed change in magnetic anisotropies in patterned (Ga,Mn)As results from anisotropic elastic strain relaxation that leads to a hard uniaxial axis perpendicular to the patterned stripe and an easy axis along the stripe.[21–23] This lithographically induced strain relaxation allows then for a local control of magnetic anisotropy in spintronic devices based on (Ga,Mn)As. This enables building devices with different switching fields for different contacts, which is necessary for efficient operation of spintronic devices, including spin-valve devices. Reference 23 presents a detailed study of lithographicaly induced anisotropies in narrow bars fabricated from 50-nm thick (Ga,Mn)As films with a Mn content of 6% grown in the same molecular beam epitaxy (MBE) machine as the material investigated in this work. It was shown that for stripe widths larger than 1.5 μm the anisotropy of the stripes resembled the one of the extended layer, i.e., was dominated by the biaxial anisotropy, whereas the lithographicaly induced uniaxial anisotropy was becoming dominant for $w_x < 1\,\mu$m. In the following we will present the results of our experimental studies on the influence of the anisotropic properties of the injecting and detecting contacts on the signal observed in spin-valve measurements in lateral spin-injection devices. We study devices with contacts oriented either along the [100] direction, i.e., cubic easy axes, as well as contacts oriented along the $[1\bar{1}0]$ direction.

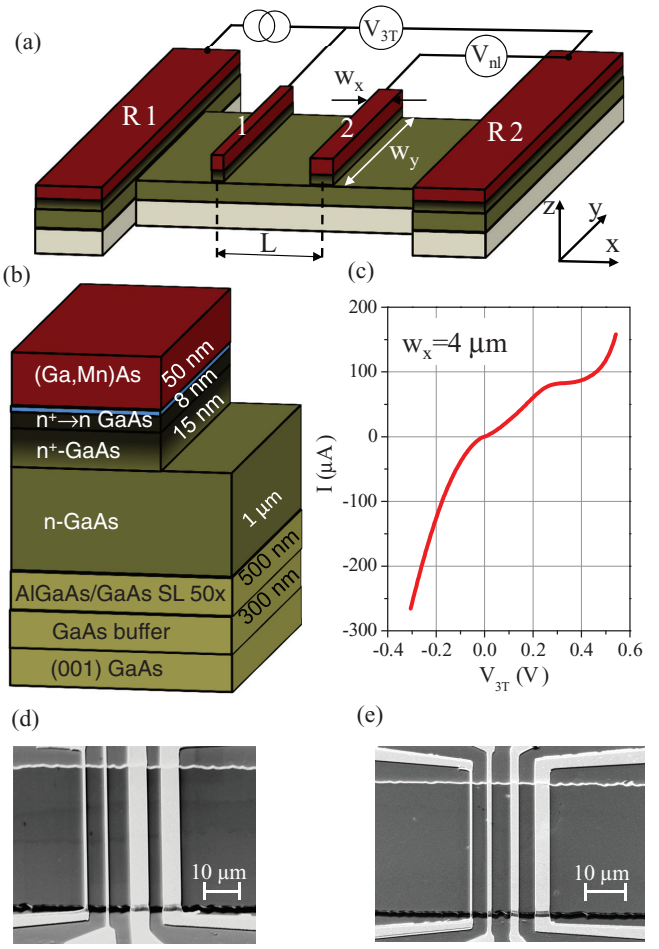

FIG. 1. (Color online) (a) Layout of a typical lateral spin-injection device with one injecting and one detecting contact, allowing for both four-terminal nonlocal (NL) and three-terminal (3T) measurements. (b) The layer sequence of the used wafer. (c) Current-voltage characteristic of the Esaki diode structure taken at a 4-μm-wide contact. (d) and (e) SEM pictures of two multiterminal devices with typical geometries of the contacts.

III. EXPERIMENTAL: DEVICES AND METHODS

A. Lateral spin-injection device

The layout of a typical nonlocal lateral spin-injection device used in our experiment is presented in Fig. 1(a). It consists of a lateral GaAs channel of a width $w_y = 50\,\mu$m and a length of 750 μm oriented along the x direction, with narrow ferromagnetic (FM) Esaki diode contacts 1 and 2, which could serve either as an injector or detector, placed above the nonmagnetic (NM) GaAs channel. Spin accumulation is generated in the channel by a charge current flowing through the FM/NM interface along the z direction, i.e., perpendicularly to the plane of the junction. This accumulation diffuses then along the channel (x direction) away from the injector (contact 1 in the picture). Due to a spin-charge coupling[24,25] it can be subsequently detected by another FM contact (contact 2), located outside of the current path. Two 150 μm $\times$150 μm sized contacts $R1, R2$ at the edges of the mesa are used as reference contacts. Although they also contain the spin Esaki diode structure, their large size results in the small ohmiclike resistance and their large separation of $\approx 350\,\mu$m from the narrow contacts in the center, much larger than a typical for our devices spin diffusion length of $\approx 5\,\mu$m, ensures that they do not influence the signal generated (or detected) by the latter. Three-terminal (3T) voltage V_{3T} constitutes a voltage drop across the interface, and can be used to monitor the magnetic behavior of the contact through the tunneling magnetoresistance (TAMR) effect.[18,19]

The layout of the molecular beam epitaxy (MBE)-grown wafer from which devices were fabricated is shown in Fig. 1(b). The wafer, grown on a semi-insulating (001) GaAs substrate, consists of the following layers (in the order of growth): 300 nm of GaAs buffer, 500 nm of GaAs/AlGaAs superlattice, 1000 nm of lightly Si-doped n-GaAs constituting the transport channel, 15 nm $n \rightarrow n^+$ transition layer with $n^+ = 5 \times 10^{18}\,\mathrm{cm}^{-3}$, and 2.2 nm $Al_{0.33}Ga_{0.67}As$ layer. These layers have been grown using a standard, high-temperature MBE process. After that the temperature has been reduced and the top layer of 50 nm (Ga,Mn)As has been grown using

low-temperature (LT) MBE growth. The top (Ga,Mn)As layer and the higher doped n-GaAs layers form the Esaki diode structure. The transport channel is first defined by fabricating a mesa using standard optical lithography and wet chemical etching with acetic acid. Then large reference contacts are defined also by optical lithography and subsequent evaporation of a Ti/Au gold layer. Narrow injecting/detecting contacts are defined using e-beam lithography and evaporation of approximately 15 nm/150 nm Ti/Au. In the last step the highly doped top layers are etched away to limit the lateral transport to the channel layer. We performed measurements on more than 15 samples fabricated from wafers with n-doping levels ranging from $n = 2 \times 10^{16}$ cm^{-3} to $n = 6 \times 10^{16}$ cm^{-3} and Mn content between 5% and 6%. Most of the experimental results presented here were obtained from the wafer with $n = 6 \times 10^{16}$ cm^{-3} and Mn content of 6%. In Figs. 1(d) and 1(e) we show SEM pictures of two typical multicontact devices we have studied, featuring contacts with different sizes. The length of the contacts is always equal to the width of the mesa $w_y = 50\ \mu$m, whereas the width of the contacts w_x is varied. The SEM pictures show devices featuring two 0.5-μm-wide contacts with two 4-μm-wide contacts (d) and four contacts with widths of 0.5, 1, 2, and 4 μm (e). The functionality of the Esaki diode is shown in Fig. 1(c), where we plot the current-voltage characteristic of the Esaki diode contact of size $4 \times 50\ \mu$m^2, with the voltage drop V_{3T} measured across the interface using the 3T configuration. An efficient Esaki diode operation is confirmed by a dip at about $0.4V$ in the I-U characteristic, typical for tunnel diodes.[26]

B. Spin-valve effect

The nonlocal spin-valve (NLSV) measurement is a standard way of the electrical detection of injected spins.[1,2,12] The typical measurement configuration is shown in Fig. 1(a). Current is injected between contacts $1 - R1$ and the generated spin accumulation is detected as a nonlocal voltage between contact 2 and the reference contact $R2$. In a typical SV measurement an external in-plane magnetic field B is swept along the long axis of the contacts, i.e., in the y direction in our case, and the switching in the nonlocal voltage is observed as a result of the reorientation of the magnetization in the injecting and detecting contacts during a magnetization reversal process. According to the standard model of spin injection[25,27] the nonlocal voltage $V_{\rm nl}^s$ is a measure of a spin accumulation and given by

$$V_{\rm nl}^s = \pm P_{\rm inj} P_{\rm det} I R_{\rm sheet} \lambda_{\rm sf}/2w \times \exp(-L/\lambda_{\rm sf}), \qquad (1)$$

where I is the injection charge current, $R_{\rm sheet}$ and $\lambda_{\rm sf}$ are, respectively, the sheet resistance and the spin diffusion length in the channel, $P_{\rm inj(det)}$ is the spin-injection (detection) efficiency being expressed by the spin polarization of the current flowing through a given contact, and L is the distance between injector and detector contact. The plus (minus) sign corresponds to the case of the parallel (antiparallel) configuration of the magnetizations in injector and detector contacts. An experimentally measured nonlocal voltage is given by $V_{\rm nl} = V_{\rm nl}^s + V_{\rm nl}^{\rm offset}$, where $V_{\rm nl}^{\rm offset}$ is an offset voltage measured commonly in nonlocal devices,[12] particularly in those with a semiconducting channel,[1,2,28] and partially assigned to thermoelectric effects.[29] In all our experiments we performed field sweeps from $+0.5\ T$ down to $-0.5\ T$ and back, as this field was strong enough to orient the magnetization of the (Ga,Mn)As stripes along the external field direction.

In order to analyze SV traces in terms of magnetic anisotropy properties it is necessary to separately determine the switching fields of the involved single contacts. For this purpose we measured also the resistance of each single contact in three-terminal (3T) configuration while sweeping B_y and monitoring the voltage drop across the interface V_{3T}. Due to the TAMR effect occurring in FM/GaAs junctions the resistance of the contact depends on the absolute magnetization orientation in the ferromagnet, in our case in the (Ga,Mn)As stripe.[18,19] Any reorientation of magnetization while sweeping the magnetic field results then in a change of V_{3T}. In our analysis we neglected the possible influence of stray magnetic fields of the ferromagnetic contacts onto each other, as we did not observe any dependence of the observed switching pattern on the distance between injector and detector. This is fully expected given the small value of demagnetizing fields in (Ga,Mn)As.

C. Hanle effect

The other very important type of measurement commonly used to study spin accumulation is a measurement of the Hanle effect,[1,2,25,30,31] i.e., the precession and dephasing of the injected spins during transport between the injector and the detector in an external magnetic field B perpendicular to the plane of the sample, i.e., also to the initial orientation of the injected spins, the latter being collinear with the magnetization of the injecting contact. As the detector is sensitive to a spin projection on its own magnetization axis, the precession of spins results in an oscillating $V_{\rm nl}^s$, while dephasing and the following depolarization result in a decay of the spin signal until $V_{\rm nl}^s = 0$. Because of the latter, Hanle measurements can be used to determine the offset voltage $V_{\rm nl}^{\rm offset}$. The following procedure was employed to perform the measurements. First the magnetization of the contacts was saturated by applying $B_y = 0.5\ T$ and the field was then swept to zero. Subsequently the sample was rotated out of plane by 90° and the field was swept perpendicularly to the sample plane up to $B_z = 0.5\ T$ in order to induce the Hanle effect. After that the sample was rotated back to the previous position and the procedure was repeated, with sweeping B_z in the opposite direction, i.e., down to $B_z = -0.5\ T$. Thus we avoided sweeping B_z through zero because of the strong effects related to dynamic nuclear polarization (DNP)[32–35] induced by injected electron spins. For the same reason we also waited approximately 10 min after sweeping B_y to zero and before sweeping B_z, allowing the resulting nuclear field to relax.[35]

To analyze the measured experimental curves we employed in our study a model developed in Ref. 25. Following that model, a magnetic-field-dependent nonlocal voltage $V_{\parallel}(B_z)$ and $V_{\perp}(B_z)$, measured at the detector placed at x with the injector at $x = 0$ for, respectively, parallel and orthogonal configuration of the magnetization of injector and detector

contact, can be expressed by

$$V_{\parallel}(B_z) = V_0 \exp(-\alpha_1 x/\lambda_{sf}) \times \left[\frac{2\kappa + \alpha_1}{(2\kappa + \alpha_1)^2 + \alpha_2^2} \cos\left(\frac{\alpha_2}{\lambda_{sf}} x\right) - \frac{\alpha_2}{(2\kappa + \alpha_1)^2 + \alpha_2^2} \sin\left(\frac{\alpha_2}{\lambda_{sf}} x\right) \right], \quad (2a)$$

$$V_{\perp}(B_z) = V_0 \exp(-\alpha_1 x/\lambda_{sf}) \times \left[\frac{2\kappa + \alpha_1}{(2\kappa + \alpha_1)^2 + \alpha_2^2} \sin\left(\frac{\alpha_2}{\lambda_{sf}} x\right) + \frac{\alpha_2}{(2\kappa + \alpha_1)^2 + \alpha_2^2} \cos\left(\frac{\alpha_2}{\lambda_{sf}} x\right) \right], \quad (2b)$$

where V_0 is the voltage that would be detected at the injection point $x = 0$ and κ is the parameter describing the influence of drift on the obtained curve (in our case $\kappa = 0$). The parameters α_1 and α_2 are given by $\alpha_1 = (1/\sqrt{2})\sqrt{1 + \kappa^2 + \sqrt{(1 + \kappa^2) + (\omega_L \tau_s)^2}} - \kappa$ and $\alpha_2 = \mathrm{sgn}(\omega_L)(1/\sqrt{2})\sqrt{-1 - \kappa^2 + \sqrt{(1 + \kappa^2) + (\omega_L \tau_s)^2}}$ where ω_L and τ_s are, respectively, the Larmor frequency $\omega_L = g\mu_0 B_z/\hbar$ and the spin relaxation time. To take finite dimensions of the employed contacts into account the experimental data were fitted with Eq. (2) integrated along x over the width of the injector and the detector.

IV. RESULTS AND DISCUSSION

A. Contacts along [100]

As described in Sec. II, both [100] and [010] crystallographic directions constitute magnetic cubic easy axes in extended (Ga,Mn)As layers and remain easy also for stripe widths down to $w_x \approx 1.5\ \mu$m.[23] For narrower stripes an anisotropic strain relaxation induces a strong uniaxial anisotropy with an easy axis along the y direction. In the following we show results of SV measurements for three different geometrical configurations, which we name narrow-narrow, narrow-wide, and wide-wide, where by *narrow* we mean a contact showing uniaxial anisotropy and *wide* is a contact with biaxial anisotropy.

In Fig. 2 we show typical results of SV measurements for the narrow-narrow configuration, i.e., for injector and detector widths $w_{\mathrm{inj}} = 0.5\ \mu$m and $w_{\mathrm{det}} = 1\ \mu$m, respectively, and the injection current $I = -2\ \mu$A. In the top and bottom panel of Fig. 2 we show V_{3T} measured, respectively, at injector contact 1 (top) and detector contact 2 (bottom), whereas in the middle panel we plot V_{nl}. We can clearly see single switching events in the V_{3T} curves owing to the magnetic reversal, consistent with the claim that long axes of the contacts are indeed magnetic easy axes. The B-field positions of these features in the V_{3T} curves match exactly the switching fields observed in the SV signal seen in the middle panel: a lower switching field for $w_x = 1\ \mu$m and larger for $w_x = 0.5\ \mu$m. The measured SV curve shows a fully expected pattern: The nonlocal signal jumps whenever the alignment of the injector's and detector's magnetization switches from parallel to antiparallel and back (line corresponding to $V^s = 0$ was determined from Hanle measurements, shown in Fig. 3). The amplitude of the signal is $\Delta V_{\mathrm{nl}}^{sv} = 2V_{\mathrm{nl}}^{s}$, with V_{nl}^{s} given by Eq. (1). A sharp feature seen at $B_y = 0$ is commonly observed in GaAs-based spin-injection

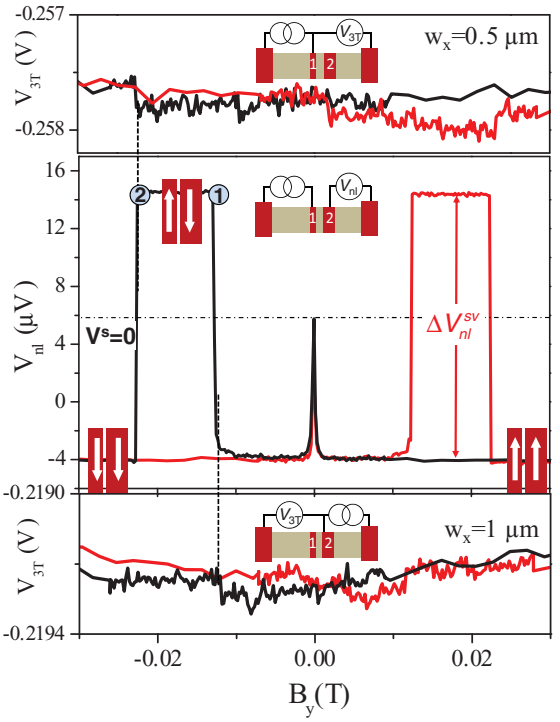

FIG. 2. (Color online) Typical results of in-plane B sweeps for the narrow injector and detector contacts oriented along the [100] direction. (Middle panel) NLSV curve for $w_{\mathrm{inj}} = 0.5\ \mu$m and $w_{\mathrm{det}} = 1\ \mu$m and for $I_{\mathrm{inj}} - 2\ \mu$A. (Top and bottom panel) 3T voltage for 0.5-μm- and 1-μm-wide contacts, for the current of $-2\ \mu$A and $-5\ \mu$A, respectively. Black and red curves correspond to down and up sweeps of magnetic field, respectively. For the down-sweep curves we mark switching events and sketch the corresponding magnetization configuration in both contacts. The zero-spin-signal level $V_{\mathrm{nl}}^{s} = 0$ is also indicated, as determined from Hanle measurements; see Fig. 3.

devices[1,2,28] and originates from dynamic nuclear polarization (DNP) effects.[32,33,35] From SV measurements performed for different injector–detector separations we determined, using Eq. (1), the spin-diffusion length $\lambda_{sf} = 5.7\ \mu$m and the spin-injection efficiency $P = \sqrt{P_{\mathrm{inj}} P_{\mathrm{det}}} = 75\%$.

In Fig. 3 we show results of Hanle measurements conducted for the configuration corresponding to the top (AP) and to the bottom (P) of the spin-valve feature, as marked in the figure by a blue and a red dot. The resulting curves are symmetric with respect to $B = 0$, as expected for a collinear orientation of the magnetization in injector and detector contacts. The maximum signal $\Delta V_{\mathrm{nl}}^{\mathrm{Hanle}}$ occurs at zero field, but then decreases as a result of spin precession and dephasing in a transverse magnetic field. Because the spin-related signal V^s vanishes at large magnetic fields, one can extract from these measurements the value of the offset voltage $V^{\mathrm{offset}} = 5.2\ \mu$V. As expected, the amplitude of the observed signal $\Delta V_{\mathrm{nl}}^{\mathrm{Hanle}}$ is half of the amplitude of the spin-valve signal $\Delta V_{\mathrm{nl}}^{\mathrm{sv}}$ observed for AP-P switching. The solid lines are theoretical curves obtained from Eq. (2a) for $P = \sqrt{P_{\mathrm{inj}} P_{\mathrm{det}}} = 75\%$, $\lambda_{\mathrm{sf}} = 5.7\ \mu$m, and the spin relaxation time $\tau_s = 30$ ns, i.e., parameters fully consistent with our SV measurements. It is interesting to note, however, that at low-field values the experimental curves are slightly narrower then the theoretical ones. The reason

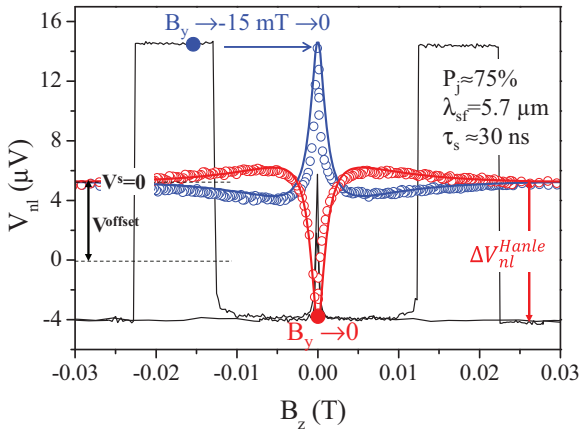

FIG. 3. (Color online) Typical results of the Hanle experiment for the same measurement configuration as in Fig. 2 (NLSV signal shown also for comparison). Red and blue colors correspond to parallel (P) and antiparallel (AP) initial configuration of magnetizations, realized by B sweeps in the y direction as marked in the figure. Symbols represent the experimental data and solid lines correspond to fits with Eq. (2a) for given parameters. Shown also is the zero-spin-signal level $V_{\rm nl}^s = 0$.

for this is a DNP-related magnetic field that adds up to the externally applied field narrowing the experimentally observed curves.[2,34]

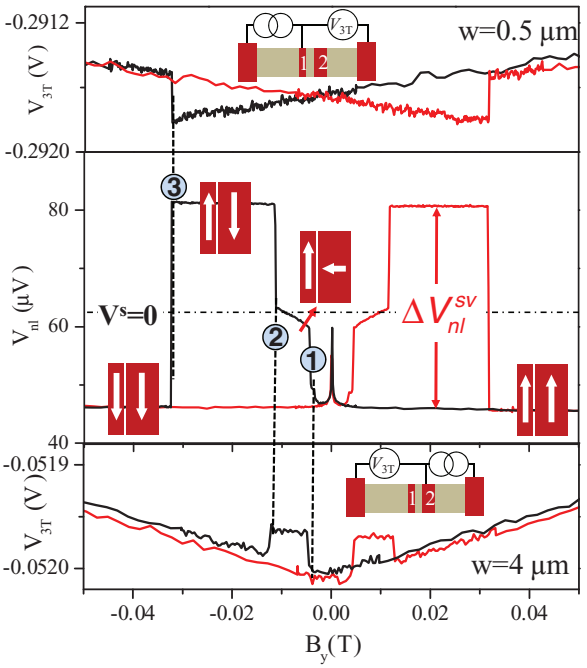

FIG. 4. (Color online) Typical results of in-plane sweeps for the narrow injector and the wide detector contacts oriented along the [100] direction. (Middle panel) NLSV curve for $w_{\rm inj} = 0.5\ \mu$m, $w_{\rm det} = 4\ \mu$m, and $I_{\rm inj} = -5\ \mu$A. (Top and bottom panel) 3T voltage for 0.5-μm- and 4-μm-wide contacts, for current of $-5\ \mu$A. Black and red curves correspond to down and up sweeps of magnetic field, respectively. For the down-sweep curve we mark switching events and sketch the corresponding magnetization configurations in both contacts. The zero-spin-signal level $V_{\rm nl}^s = 0$ is also indicated, as determined from the Hanle measurements; see Fig. 5.

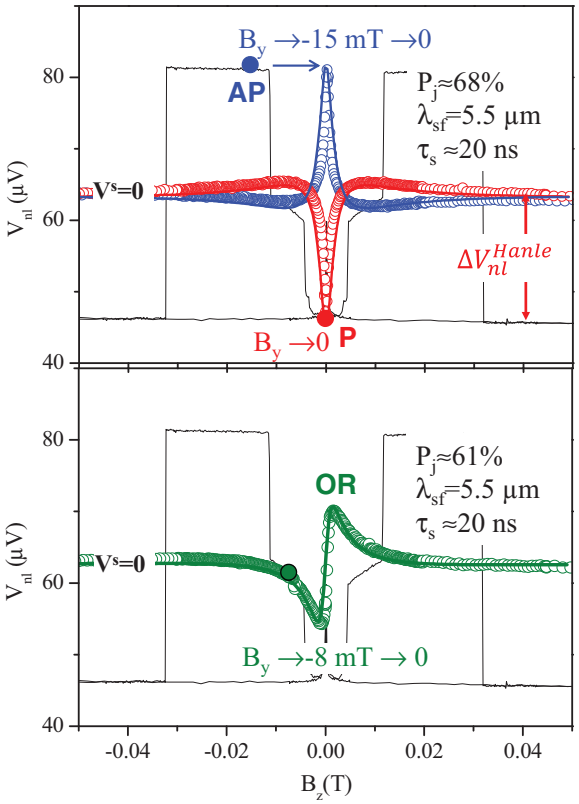

FIG. 5. (Color online) Typical results of the Hanle experiment for the same measurement configuration as in Fig. 4 (NLSV signal shown also for comparison). (Top panel) Parallel (P, red) and antiparallel (AP, blue) initial configuration of magnetization; (bottom panel) the orthogonal configuration of magnetization. Initial configurations of magnetization realized by B sweeps in the y direction as marked in the figure. Symbols represent the experimental data and solid lines correspond to fits with Eq. (2) for the parameters given above. Shown also is the zero-spin-signal level $V_{\rm nl}^s = 0$.

The measured pattern changes dramatically when we increase the size of one of the contacts used in the measurements. In Fig. 4 we show a typical SV signal for the narrow-wide configuration. Instead of two switching events, like in the case of the AP-P switching, we do observe three such features. Comparing the measured curve with V_{3T} we assign the two low-field switching events 1 and 2 to the wide detector contact and the high field switching 3 to the narrow injector contact. Only during this latter switching event $V_{\rm nl}^s$ changes its sign ($V_{\rm nl}^s = 0$ line determined from Hanle measurements shown in Fig. 5), allowing one to assign this event to AP-P switching, as it is further confirmed by the Hanle measurements performed at the top and bottom of the spin-valve feature (see the top panel of Fig. 5).

In region 1–2, on the other hand, the signal approaches $V_{\rm nl}^s = 0$. In order to gain more information about the origin of this behavior we performed Hanle measurements for the discussed configuration (shown in the bottom panel of Fig. 5) with B_z sweeps performed after B_y was swept from 0.5 T down to -8 mT (marked with a green dot) and then back to zero field. We observe in this case an antisymmetric behavior of the signal, characteristic for an orthogonal configuration of the magnetization in the injector and in the detector. The

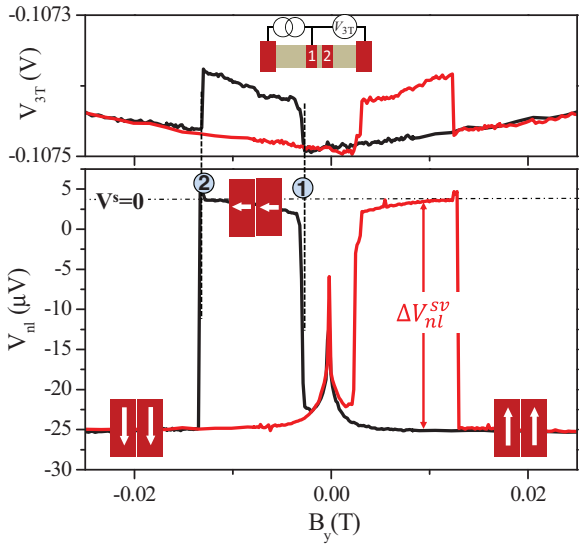

FIG. 6. (Color online) Typical results of in-plane sweeps for wide injector and detector contacts (both $w_x = 4\ \mu$m) oriented along the [100] direction. (Bottom panel) NLSV curve for a current of $-10\ \mu$A. (Top panel) 3T voltage at the injector contact. Black and red curves correspond to down and up sweeps of magnetic field, respectively. For the down-sweep curve we mark switching events and sketch the corresponding magnetization configurations in both contacts. The zero-spin-signal level $V^s_{\rm nl} = 0$ is also indicated, as determined from the Hanle measurements; see Fig. 7.

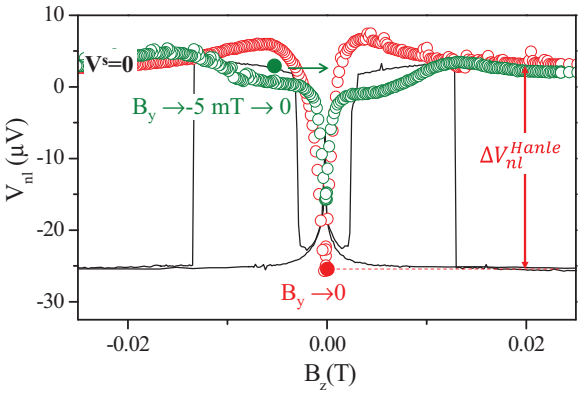

FIG. 7. (Color online) Typical results of the Hanle experiments for the same measurement configuration as in Fig. 6 (NLSV signal shown also for comparison) for two different initial magnetization configurations, realized by B sweeps in the y direction, as marked in the figure. Indicated is also the zero-spin-signal level $V^s_{\rm nl} = 0$.

experimental data can be well fitted with Eq. (2b) using the parameters shown in Fig. 5. The origin of this orthogonal configuration can be explained by a double step magnetization reversal process in the wide contact through nucleation and propagation of a 90° domain wall. When the magnetic field is swept from 0.5 T down, the magnetization switches at position 1 (see Fig. 4) from being aligned along the $B_y \| [100]$ direction towards $x \| [010]$, whereas the magnetization of the narrow injector remains aligned along the [100] direction. As a result at $B = 0$ the magnetization of the detector is perpendicular to the injected spins, i.e., $V^s_{\rm nl} = 0$, because the detector contact detects only the projection of the spin on its own magnetization axis. Finite B_z induces precession of spins, so they acquire a component collinear with the magnetization of detector, which results in a finite value of $V^s_{\rm nl}$. In a higher magnetic field spins become depolarized and therefore the measured spin signal approaches zero. At position 2 in the B_y sweep the magnetization of the wide contact switches by another 90° completing its reversal. It is now antiparallel to the magnetization of the injector. The latter reverses in one step at the position 3 and both magnetizations are now parallel to each other and to the external magnetic field.

Let us finally discuss the wide-wide configuration. In Fig. 6 we show the results of SV measurements when both the injector and the detector have a width of 4 μm. The V_{3T} signal for such contacts shows a double step reversal, with switching occurring at the same magnetic field values for both contacts. As a result, the contacts are always parallel, never reaching the AP configuration. The SV-like signal is, however, still observed for such a configuration. We explain it as follows. While sweeping the field from 0.5 T down, the magnetization in both contacts switches at point 1 by 90°. In region 1–2 the injected spins are now parallel to the detector but perpendicular to the external magnetic field. As a result, they do precess around this transverse field and become depolarized, which in turn leads to $V^s_{\rm nl} = 0$. At the position 2 the magnetization switches by another 90° completing its reversal, i.e., aligning itself again along the external B_y and the finite value of the spin signal is restored. The parallel orientation of the magnetizations is confirmed by Hanle measurements in both discussed configurations, shown in Fig. 7. We attribute the observed small asymmetry of the measured signals to the DNP effects. These are particularly strong for a configuration realized at the top of the SV signal. This can be explained by the fact that the nuclear B_N field, originating from nuclear spins polarized initially in the y direction, is in this configuration perpendicular to the injected electron spins. This results also in a reduced spin signal at $B = 0$.

These results are fully consistent with our original studies reported in Ref. 2, where the experiments were performed in such a wide-wide configuration and the SV-like pattern due to switching of $V^s_{\rm nl}$ to zero was also observed. Based on our current investigations we conclude that the latter did not originate from the formation of multidomain structures in (Ga,Mn)As contacts, as we previously speculated, but it was caused by the mechanism described above, instead. The fact that the contacts in those other devices showed double-step magnetization reversal, despite their narrow sizes ($1 \times 10\ \mu$m^2), is ascribed to a reduced (Ga,Mn)As layer thickness of 20 nm (Mn content, 5%) grown on the 250-nm-thick GaAs channel. This is expected to result in different strain relaxation for those contact stripes and slightly different anisotropy properties, compared to the wafers used here.

B. Contacts along [1$\bar{1}$0]

Although [1$\bar{1}$0] directions constitute hard cubic axis in (Ga,Mn)As, we did perform in the past successful SV experiments on devices with contacts oriented along this direction.[36] Typical spin-valve measurements are shown in Fig. 8 for the narrow injector and the wide detector contact.

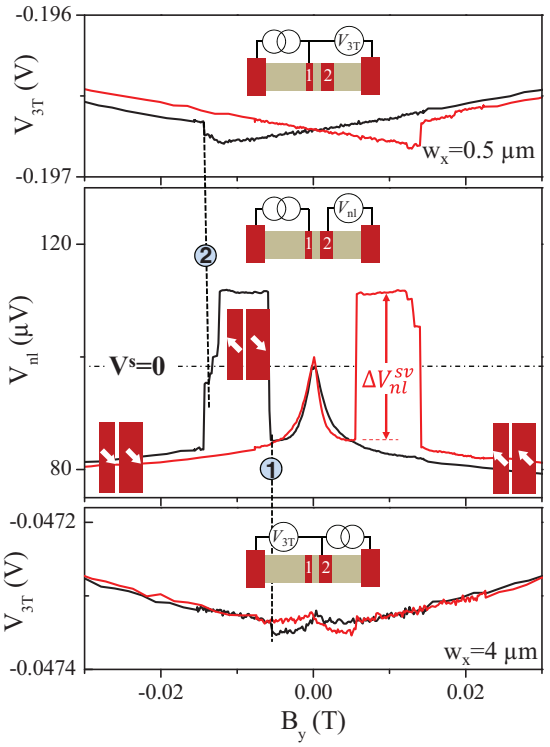

FIG. 8. (Color online) Typical results of in-plane sweeps for narrow injector and wide detector contacts oriented along $[1\bar{1}0]$ direction. (Middle panel) NLSV curve for $w_{\mathrm{inj}} = 0.5\ \mu$m and $w_{\mathrm{det}} = 4\ \mu$m for $I_{\mathrm{inj}} = -10\ \mu$A. (Top and bottom panel) 3T voltage for 0.5-μm- and 4-μm-wide contacts for $I_{\mathrm{inj}} = -10\ \mu$A. Black and red curves correspond to down and up sweeps of magnetic field, respectively. For the down-sweep curve we mark switching events and sketch corresponding magnetization configurations in both contacts. The zero-spin-signal level $V_{\mathrm{nl}}^{s} = 0$ is also indicated, as determined from the Hanle measurements; see Fig. 9.

One can see that both contacts show the one step reversal, with the narrow contact switching at higher magnetic field. We observed such a behavior for all studied contact widths, i.e., we never observed a double switching for this contact orientation. As the measured NL voltage switches symmetrically around $V_{\mathrm{nl}}^{s} = 0$ (determined using Hanle measurements; see Fig. 9) we can assign the observed features to the P-AP switching. From the measurements we get also $\Delta V_{\mathrm{nl}}^{\mathrm{Hanle}} > 1/2 V_{\mathrm{nl}}^{\mathrm{sv}}$, i.e., different from the cases discussed before for [100]-oriented contacts. As a result, the spin-injection efficiency obtained from Hanle measurements is, with $P \approx 80\%$, higher than the value of 65% obtained from SV measurements. We can explain such a behavior presuming that the magnetization in both contacts does not orient along the long axis of the contacts but instead forms a certain angle with it and also with the external magnetic field B_y. As a result, the injected spins are subjected to the transverse component of the external magnetic field. This component partially depolarizes them, thus decreasing the amplitude of the measured SV signal. Hanle measurements are performed while sweeping the magnetic field starting at $B = 0$, i.e., without any in-plane transverse field component.

The above interpretation can be confirmed by comparing measurements in this configuration ($B \| y \| [1\bar{1}0]$) with those performed for contacts along the [100] direction when B

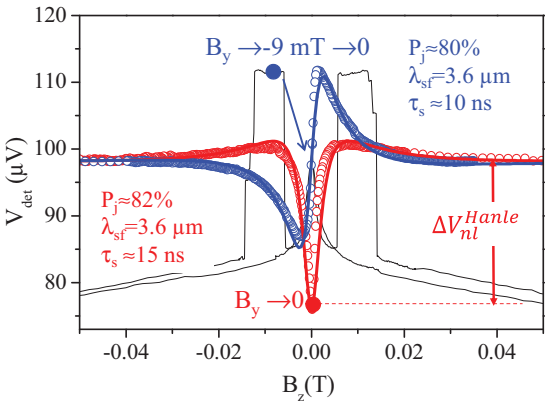

FIG. 9. (Color online) Typical results of Hanle experiments for the same measurement configuration as in Fig. 8 (NLSV signal shown also for comparison) for two different initial magnetization configurations, realized by B sweeps in the y direction as marked in the figure. Indicated also is a zero-spin-signal level $V^{s} = 0$.

is swept at the angle of -45° to the contact ($y \| [100]$ and $B \| [1\bar{1}0]$). Corresponding graphs are plotted in Fig. 10. One can clearly see the similarity between V_{3T} traces, as well as between NLSV traces, measured in both these configurations. In the V_{3T} curves kinks at $\approx \pm 0.15\ T$ are observed. They can be assigned to the field where the magnetization orients itself along the applied external magnetic field. At these points the measured nonlocal voltage V_{nl}^{s} reaches its maximum value $V_{\mathrm{nl}}^{s,\mathrm{max}}$, corresponding to the case where the magnetization of both contacts are oriented along the external field. No such feature was observed for an earlier discussed $B \| y \| [100]$ configuration (shown in top panel of Fig. 10). Both the spin-diffusion length $\lambda_{\mathrm{sf}} = 4.2\ \mu$m and the spin-injection efficiency

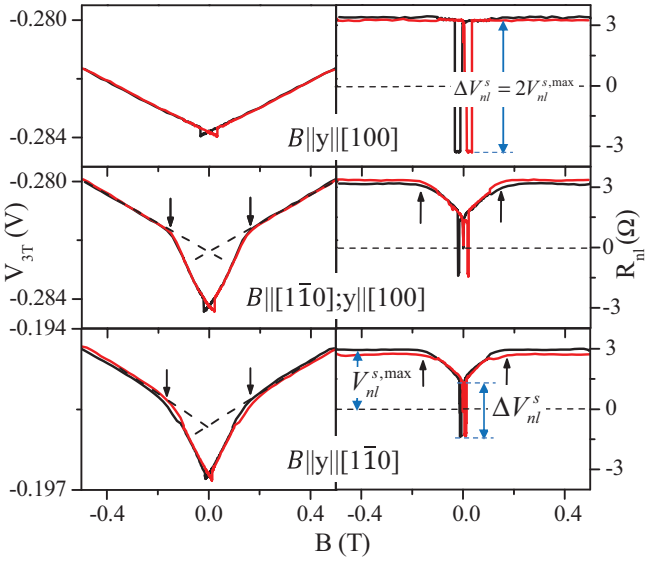

FIG. 10. (Color online) Comparison of SV signals, plotted as the nonlocal resistance $R_{\mathrm{nl}} = V_{\mathrm{nl}}^{s}/I_{\mathrm{inj}}$ in a wide range of magnetic field, for three different measurement configurations, as labeled in the figure, with injector–detector separation $L = 5.25\ \mu$m in all three cases. Arrows indicate B-field values at which magnetization vectors in both contacts orient themselves along the external magnetic field.

$P \approx 80\%$ calculated from the dependence of $V_{\mathrm{nl}}^{s,\mathrm{max}}$ on the injector-detector separation are slightly larger than values of $\lambda_{\mathrm{sf}} = 3.6\ \mu$m and $P \approx 65\%$ obtained from $\Delta V_{\mathrm{nl}}^{s}$, consistent with the picture of the spin accumulation being partially depolarized by the transverse magnetic field. It is worth also noting that the value of $V_{\mathrm{nl}}^{s,\mathrm{max}}$ is similar to the one measured for the $B \| y \| [100]$ case.

The very good quantitative and qualitative agreement between the measurements in the $y \| [100]$, $B \| [1\bar{1}0]$, and the $B \| y \| [1\bar{1}0]$ configurations suggests that the magnetic reversal process is similar in both cases. We conclude therefore that in the case of contacts oriented along the $[1\bar{1}0]$ direction the biaxial anisotropy is dominant and the easy axis is not oriented along the long axis of the contacts but rather along cubic [100] axes, at least for contact widths investigated in our study, i.e., down to the width of 0.5 μm. Interestingly, however, the AP configuration is not stable upon decreasing magnetic field down to zero, as is shown by Hanle measurements; see Fig. 9. Antisymmetric shape of the curve obtained in those measurements points clearly towards an orthogonal configuration.

V. CONCLUSIONS

To summarize our findings, we can say that the rich anisotropy of (Ga,Mn)As has a profound effect on the SV signal observed in lateral devices with (Ga,Mn)As/GaAs Esaki diodes as spin injecting/detecting contacts. The strain-induced local anisotropy control technique can be used to successfully tune the coercive fields of the involved contacts, however, one has to carefully design the devices, paying particular attention to their geometry. To realize a clear parallel-antiparallel switching in devices with contacts along a [100] direction one has to fabricate devices with at least one of the contacts in the submicron regime. One can, however, observe a spin-valve-like signal also for devices with wider contacts, which reorient their magnetization in two 90° steps during a magnetic reversal process. In the range of magnetic field where the magnetization of such a (Ga,Mn)As contact is switched by 90° with a reference to its initial direction a detected spin signal vanishes, due to the orthogonal orientation of the magnetization and the injected spins (the wide detector case) or as a result of depolarization of the injected spins by the external in-plane field (the wide injector case). This results in a nonlocal spin-valve-like signal, with its amplitude being half of that observed for P–AP switching.

Alternatively one can orient contacts along the $[1\bar{1}0]$ direction, where the AP-P switching, in field sweeps along the long axis of the contacts, can be observed even for 4-μm-wide (Ga,Mn)As stripes.[36] One has to, however, take into account that the measured signal in that case corresponds to the spins injected along [100] directions, which are partially depolarized by magnetic field $B \| [1\bar{1}0]$. Nevertheless, this geometry could be particularly useful in studying of the spin injection in a local configuration, where a spin signal is expected to be proportional to w_x/t where w_x is the contact width and t is the thickness of the channel.[37]

ACKNOWLEDGMENT

This work has been supported by Deutsche Forschungsgemeinschaft (DFG) through Project No. SFB689.

*mariusz.ciorga@ur.de

[1] X. Lou, C. Adelmann, S. A. Crooker, E. S. Garlid, J. Zhang, K. S. M. Reddy, S. D. Flexner, C. J. Palmström, and P. A. Crowell, Nat. Phys. **3**, 197 (2007).
[2] M. Ciorga, A. Einwanger, U. Wurstbauer, D. Schuh, W. Wegscheider, and D. Weiss, Phys. Rev. B **79**, 165321 (2009).
[3] S. P. Dash, S. Sharma, R. S. Patel, M. P. de Jong, and R. Jansen, Nature (London) **462**, 491 (2009).
[4] K.-R. Jeon, B.-C. Min, Y.-H. Jo, H.-S. Lee, I.-J. Shin, C.-Y. Park, S.-Y. Park, and S.-C. Shin, Phys. Rev. B **84**, 165315 (2011).
[5] H. Ohno, A. Shen, F. Matsukura, A. Oiwa, A. Endo, S. Katsumoto, and Y. Iye, Appl. Phys. Lett. **69**, 363 (1996).
[6] H. Ohno, Science **281**, 951 (1998).
[7] A. Einwanger, M. Ciorga, U. Wurstbauer, D. Schuh, W. Wegscheider, and D. Weiss, Appl. Phys. Lett. **95**, 152101 (2009).
[8] B. Endres, M. Ciorga, M. Schmid, M. Utz, D. Bougeard, D. Weiss, G. Bayreuther, and C. Back, Nat. Commun. **4**, 2068 (2013).
[9] M. Kohda, Y. Ohno, K. Takamura, F. Matsukura, and H. Ohno, Jpn. J. Appl. Phys. **40**, L1274 (2001).
[10] E. Johnston-Halperin, D. Lofgreen, R. K. Kawakami, D. K. Young, L. Coldren, A. C. Gossard, and D. D. Awschalom, Phys. Rev. B **65**, 041306 (2002).
[11] P. V. Dorpe, Z. Liu, W. V. Roy, V. F. Motsnyi, M. Sawicki, G. Borghs, and J. D. Boeck, Appl. Phys. Lett. **84**, 3495 (2004).
[12] F. J. Jedema, A. T. Filip, and B. J. van Wees, Nature (London) **410**, 345 (2001).
[13] C. Gould, S. Mark, K. Pappert, R. G. Dengel, J. Wenisch, R. P. Campion, A. W. Rushforth, D. Chiba, Z. Li, X. Liu, W. V. Roy, H. Ohno, J. K. Furdyna, B. Gallagher, K. Brunner, G. Schmidt, and L. W. Molenkamp, New J. Phys. **10**, 055007 (2008).
[14] J. Zemen, J. Kucera, K. Olejnik, and T. Jungwirth, Phys. Rev. B **80**, 155203 (2009).
[15] G. Xiang, A. W. Holleitner, B. L. Sheu, F. M. Mendoza, O. Maksimov, B. Stone, P. Schiffer, D. D. Awschalom, and N. Samarth, Phys. Rev. B **71**, 241307 (2005).
[16] M. Sawicki, F. Matsukura, A. Idziaszek, T. Dietl, G. M. Schott, C. Ruester, C. Gould, G. Karczewski, G. Schmidt, and L. W. Molenkamp, Phys. Rev. B **70**, 245325 (2004).
[17] M. Birowska, C. Sliwa, J. A. Majewski, and T. Dietl, Phys. Rev. Lett. **108**, 237203 (2012).
[18] C. Gould, C. Rüster, T. Jungwirth, E. Girgis, G. M. Schott, R. Giraud, K. Brunner, G. Schmidt, and L. W. Molenkamp, Phys. Rev. Lett. **93**, 117203 (2004).
[19] M. Ciorga, M. Schlapps, A. Einwanger, S. Geissler, J. Sadowski, W. Wegscheider, and D. Weiss, New J. Phys. **9**, 351 (2007).
[20] R. P. Cowburn, S. J. Gray, J. Ferré, J. A. C. Bland, and J. Miltat, J. Appl. Phys. **78**, 7210 (1995).
[21] J. Wenisch, C. Gould, L. Ebel, J. Storz, K. Pappert, M. J. Schmidt, C. Kumpf, G. Schmidt, K. Brunner, and L. W. Molenkamp, Phys. Rev. Lett. **99**, 077201 (2007).

[22]J. Wunderlich, A. C. Irvine, J. Zemen, V. Holý, A. W. Rushforth, E. De Ranieri, U. Rana, K. Výborný, J. Sinova, C. T. Foxon, R. P. Campion, D. A. Williams, B. L. Gallagher, and T. Jungwirth, Phys. Rev. B **76**, 054424 (2007).

[23]F. Hoffmann, G. Woltersdorf, W. Wegscheider, A. Einwanger, D. Weiss, and C. H. Back, Phys. Rev. B **80**, 054417 (2009).

[24]M. Johnson and R. H. Silsbee, Phys. Rev. Lett. **55**, 1790 (1985).

[25]J. Fabian, A. Matos-Abiague, C. Ertler, P. Stano, and I. Žutić, Acta Phys. Slov. **57**, 565 (2007).

[26]M. S. Sze, *Physics of Semiconductor Devices* (John Wiley & Sons, New York, 1981).

[27]A. Fert and H. Jaffrès, Phys. Rev. B **64**, 184420 (2001).

[28]G. Salis, A. Fuhrer, R. R. Schlittler, L. Gross, and S. F. Alvarado, Phys. Rev. B **81**, 205323 (2010).

[29]F. L. Bakker, A. Slachter, J.-P. Adam, and B. J. van Wees, Phys. Rev. Lett. **105**, 136601 (2010).

[30]M. Johnson and R. H. Silsbee, Phys. Rev. B **37**, 5326 (1988).

[31]F. J. Jedema, H. B. Heersche, A. T. Filip, J. J. A. Baselmans, and B. J. van Wees, Nature (London) **416**, 713 (2002).

[32]G. Salis, A. Fuhrer, and S. F. Alvarado, Phys. Rev. B **80**, 115332 (2009).

[33]M. K. Chan, Q. O. Hu, J. Zhang, T. Kondo, C. J. Palmstrøm, and P. A. Crowell, Phys. Rev. B **80**, 161206 (2009).

[34]C. Awo-Affouda, O. M. J. van 't Erve, G. Kioseoglou, A. T. Hanbicki, M. Holub, C. H. Li, and B. T. Jonker, Appl. Phys. Lett. **94**, 102511 (2009).

[35]J. Shiogai, M. Ciorga, M. Utz, D. Schuh, T. Arakawa, M. Kohda, K. Kobayashi, T. Ono, W. Wegscheider, D. Weiss, and J. Nitta, Appl. Phys. Lett. **101**, 212402 (2012).

[36]M. Ciorga, C. Wolf, A. Einwanger, M. Utz, D. Schuh, and D. Weiss, AIP Adv. **1**, 022113 (2011).

[37]A. Fert, J. M. George, H. Jaffrès, and R. Mattana, IEEE Trans. El. Dev. B **54**, 21 (2007).